# Structural variations and cation distributions in $Mn_{3-x}Co_xO_4$ ($0 \leq x \leq 3$) dense ceramics using neutron diffraction data

H. Bordeneuve [a], C. Tenailleau [a,*], S. Guillemet-Fritsch [a], R. Smith [b], E. Suard [c], A. Rousset [a]

[a] Institut Carnot CIRIMAT, Universite Paul Sabatier, UMR CNRS 5085, 31062 Toulouse Cedex 9, France
[b] ISIS Facility, Rutherford Appleton Laboratory, Chilton, Didcot, Oxon, OX11 0QX, UK
[c] Diffraction Group, Institut Laue-Langevin, Grenoble, France

*Article history:*
Received 12 May 2009
Received in revised form
17 November 2009
Accepted 26 November 2009
Available online 2 December 2009

*Keywords:*
Cobalt manganese oxide ceramics
Spinels
Neutron diffraction
Structure
Bond valence sum
Cation distribution
Electrical conduction

A B S T R A C T

Single phase ceramics of cobalt manganese oxide spinels $Mn_{3-x}Co_xO_4$ were structurally characterized by neutron powder diffraction over the whole solid solution range. For $x < 1.75$, ceramics obtained at room temperature by conventional sintering techniques are tetragonal, while for $x \geq 1.75$ ceramics sintered by Spark Plasma Sintering are of cubic symmetry. The unit cells, metal–metal and metal–oxygen average bonds decrease regularly with increasing cobalt content. Rietveld refinements using neutron data show that cobalt is first preferentially substituted on the tetrahedral site for $x < 1$, then on the octahedral site for increasing $x$ values. Structural methods (bond valence sum computations and calculations based on Poix's work in oxide spinels) applied to our ceramics using element repartitions and [M–O] distances determined after neutron data refinements allowed us to specify the cation distributions in all phases. $Mn^{2+}$ and/or $Co^{2+}$ occupy the tetrahedral site while $Mn^{3+}$, $Co^{2+}$, $Co^{III}$ (cobalt in low-spin state) and $Mn^{4+}$ occupy the octahedral site. The electronic conduction mechanisms in our highly densified ceramics of pure cobalt and manganese oxide spinels are explained by the hopping of polarons between adjacent $Mn^{3+}/Mn^{4+}$ and $Co^{2+}/Co^{III}$ on the octahedral sites.

## 1. Introduction

Manganese-based oxide spinels are useful in many application fields (transport, telecommunication, medicine, energy…) due to their element abundance, low cost and toxicity, and electrical characteristics. These materials are often used as negative temperature coefficient (NTC) thermistors in microelectronic systems due to their non-linear resistivity variation with temperature [1–4].

Although $MnCo_2O_4$ and $CoMn_2O_4$ powders and thin films have been the subject of various structural, electrochemical and magnetic studies, little has been done, to our knowledge, to fully characterize $Mn_{3-x}Co_xO_4$ ceramics over the whole solid solution range [5–8]. In most cases, details of the preparation method (synthesis, thermal treatment, processing) are minimal. However, it is a critical point in the control and understanding of the chemical and physical properties of these materials. For instance, there has been different cation distributions proposed in the literature for the sample $MnCo_2O_4$ [6,8–11].

Corresponding author.
*E-mail address:* tenailleau@chimie.ups-tlse.fr (C. Tenailleau).

$Co_3O_4$ is known to have the $A[B]_2O_4$ normal spinel structure (*Fd-3m* space group) in which the $Co^{2+}$ ion ($d^7$ configuration of high-spin state) in the formula units occupies the tetrahedral site, while the two $Co^{3+}$ ions ($d^6$ configuration of low-spin state), written as $Co^{III}$ from here on, occupy the octahedral site (Fig. 1) [12,13]. $Co_3O_4$ is an insulator and exhibits an antiferromagnetic behavior below 40 K. On the other side of the phase diagram under study, the crystal structure of the haussmanite $Mn_3O_4$ present a tetragonal distortion of the spinel structure (*$I4_1/amd$* space group) due the presence of $Mn^{3+}$ in the octahedral site ($d^4$ configuration of high-spin state) and the cooperative Jahn–Teller effect (see Fig. 1) [14,15]. The critical concentration of distorting ions such as $Mn^{3+}$ required in the octahedral site is close to 55% [16]. $Mn^{2+}$ ions ($d^5$ configuration of low-spin state) occupy the tetrahedral sites. $Mn_3O_4$ is an insulator and presents ferrimagnetism below 42 K [17].

Many types of cations can be inserted into the spinel crystal structure. A large variety of ionic radii and valence states can coexist in the spinel form and an element can present different oxidation states (and spin states) on the tetrahedral and/or octahedral sites [18,19]. Thus, the cation distribution in oxides of spinel structure is generally complex to identify as the valence and coordination polyhedra are depending on steric and energetic considerations that are also related to their environment [20]. The cation

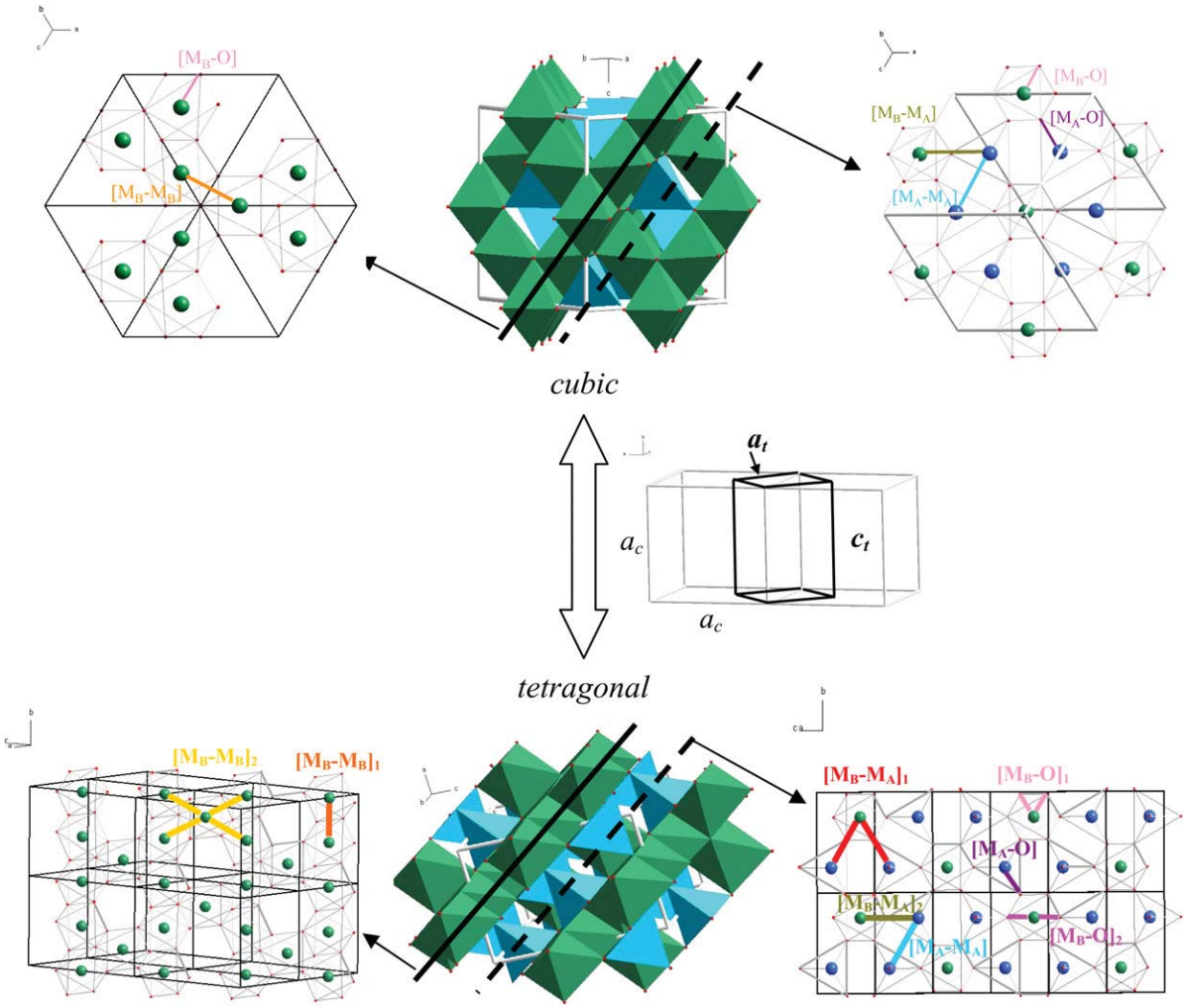


**Fig. 1.** Cubic (top) and tetragonal (bottom) spinel structures showing the succession of kagome- (left) and mixte trigonal-type (right) plans formed by the oxygen. In the former plan, only octahedral sites can be occupied by cations, while in the latter both octahedral and tetrahedral sites are available. The shortest [M–M] and [M–O] distances are represented.

with the larger radius will generally be inserted into the tetrahedral site for cations with +2 and +3 oxidation states, while it will be inserted into the octahedral site for +2 and +4 oxidation states [21]. The cation distribution in spinels is also directly influenced by the thermal treatment. For instance, the quenching of a sample at room temperature can fix a distribution that is usually out of its thermodynamic equilibrium when slowly cooled.

The electric and magnetic properties of cobalt and manganese spinel oxides are closely related to the cation arrangements and oxidation states in the two crystallographic sites. X-ray diffraction technique does not allow distinction between the cobalt and manganese elements due to their similar atomic form factors. However, neutron diffraction technique can be really useful in the determination of the cation repartition since cobalt and manganese neutron scattering lengths have different values and opposite signs. The diffraction peak intensities are particularly sensitive to the inversion parameter variations. It is therefore possible to locate each element on the tetrahedral and octahedral sites. We here report the structural variations and cation distributions of single phase and high density ceramics of $Mn_{3-x}Co_xO_4$ composition, for $0 \leq x \leq 3$, studied at room temperature. The electronic conduction mechanisms in these cobalt and manganese oxide spinels are discussed for the whole solid solution range.

## 2. Experimental

### 2.1. Preparation

In order to prepare powders of cobalt manganese oxide spinels suitable for sintering techniques, cobalt manganese oxalic precursors were obtained by the co-precipitation method of an aqueous solution of 0.2 mol $L^{-1}$ ammonium oxalate and a mixture of manganese and cobalt nitrates in the desired proportions (4 mol $L^{-1}$) [22]. After 30 min of ageing, the solution was filtered, washed several times with water and dried in air at 90 °C. A thermal decomposition in air for 4 h at 800 °C of the oxalate precursors was chosen for the formation of oxygen stoichiometric oxide powders (cooling rate of 150 °C/h). For $x = 0$, a manganese sesquioxyde was synthesized while a mixture of $(Mn,Co)_2O_3$ and a tetragonal spinel appeared for $x = 0.58$. For $0.98 \leq x < 1.78$ (compositions determined by ICP-AES measurements [22]), a mixture of tetragonal and cubic spinels were obtained, while for $1.78 \leq x \leq 3$ a single cubic spinel was formed at room temperature.

#### 2.1.1. Conventional sintering

The oxide powders were mixed with an aqueous solution of polyvinylic alcohol (17 wt%) used as a binder and pressed at

500 MPa for 30 s into 6 mm diameter pellets (height ~ 1.6 mm). Each pellet was heated to 450 °C at 40 °C/h and left for an hour before heating to the sintering temperature ($1160 \leq T \leq 1300$ °C) at 80 °C/h and held for 8 h (15 h for $Mn_3O_4$) in a muffle furnace Hermann–Moritz 2068 equipped with a West 2050 programmer, then quenched in air [22]. For $0 \leq x < 1.78$, all phases were pure tetragonal spinels. Slower cooling rates (200 °C/h down to 30 °C/h) always generated a mixture of tetragonal and cubic spinel phases. The manganese-rich oxide spinels quenched from high temperature ($T \sim 1200$ °C) often exhibited cracks in the pellets. This is not only due to the thermal shock that occurs upon abrupt cooling but also to the cell variation related to the cubic/tetragonal transition. Also, ceramics that did not show cracks to the eye after the sintering process became very brittle and finally cracked after a few weeks when left in air due to sample oxidation. Therefore, these materials were cooled down at 120 °C/h from the sintering temperature to a quenching temperature (as low as 800 °C for the Mn:Co ~ 1.5:1.5 following the $Mn_3O_4$–$Co_3O_4$ phase diagram [23]) and left for an hour before quenching in order to avoid the formation of cracks in our dense ceramics (densification > 93%). Various tests performed on $Mn_{3-x}Co_xO_4$ ceramics with $1.78 \leq x \leq 2.22$, using variable sintering temperatures, dwell times, cooling rates or oxygen partial pressures showed that it was very difficult to remove the reduced CoO phase which is formed at high temperature and that also contributes to the formation of cracks in the ceramics. We then decided to use the spark plasma sintering technique for the preparation of single phase ceramics of Co-rich manganese oxide spinels ($x \geq 1.78$).

#### 2.1.2. Spark plasma sintering (SPS)

The heating in an SPS apparatus is created by a current going through the whole sample placed in a conductive matrix and under an axial pressure. The main advantages in comparison with the conventional sintering are to lower the temperature, decrease considerably the experimental time and obtain a very high densification. The powders of $Mn_{3-x}Co_xO_4$ ($1.78 \leq x \leq 3$) were introduced in a 8 mm or 15 mm internal diameter graphite die and put under vacuum (4 Pa). The temperature was measured using a *K* thermocouple inserted within the matrix and close to the sample. The powders were sintered under 50 MPa for 5 min between 700 and 750 °C (50 °C/min heating rate), depending on the sample composition, using the Sumimoto 2080 SPS system available at the PNF2 CNRS platform at the University of Toulouse, France. Each thermal cycle took about 25 min. A series of papyex/alumina/papyex layers were put on both sides of the powder for lowering the amount of (Mn, Co)O reduced phase that appeared on the surface of the pellet during a cycle in carbon graphite. In order to remove any oxide impurities, each side of the highly densified ceramics (densification > 95%) was then polished until a single cubic spinel phase (of the same composition than the starting powder) could be identified via XRD and EDS/SEM measurements [22].

### 2.2. Characterization

Ceramics of cobalt manganese oxide spinels were first characterized by X-ray diffraction using a Bruker D4 ENDEAVOR diffractometer using Cu$K_\alpha$ radiation (40 kV, 40 mA) and a JEOL JSM 6700F scanning electron microscope (SEM) equipped with an EDX LINK analyzer. The acceleration voltage varied from 0.2 to 30 kV and the images were taken at 5 kV.

Neutron diffraction data were obtained at room temperature on Polaris at the Rutherford Appleton Laboratory, Didcot, UK, and on the Super D2B instrument available at the Institut Laue Langevin, Grenoble, France. Around 0.3–3.5 g of ceramics was ground into powders before insertion into vanadium cylinders for measurements.

The medium resolution and high intensity powder diffractometer Polaris has four detector banks that measure simultaneously: the backscattering and low angle banks using $^3$He gas tube detectors, and 90° and very low angle detector banks using ZnS scintillators. Only the time-of-flight data collected from the 58 backscattering detectors, that offer the best resolution over a large range of d-spacings (0.2–3.2°), and obtained after 30 min–2 h depending on the amount of sample, were used for structural determination. Data were normalized to the incident neutron spectrum and the detector efficiency correction was made using the VA_COR program.

Neutron diffraction patterns were also collected at room temperature with the high resolution 2D neutron detector available at the ILL. The Super D2B instrument has a 135° take-off angle and 128 $^3$He detectors. Powder diffraction patterns were recorded using a 1.5941 Å wavelength in the 10–145° $2\theta$ domain with a 0.05° step and nine scans of 200,000 × 1,2 or 4 counts.

All neutron data were analyzed for structural determination using the Rietveld method compiled with the FULLPROF program [24]. The parameters refined were, in order: scale factor, first terms of the background, zero shift, cell parameters, peak shape factors, atomic positions, thermal factors, absorption coefficient and site occupancies. An important remark is that refinements performed on $Mn_{1.25}Co_{1.75}O_4$ samples (or $x = 1.78$ as determined by ICP-AES measurements [22]) prepared by conventional and SPS techniques showed identical structural results as well as those obtained for $Mn_{0.78}Co_{2.22}O_4$ sample data recorded on both Polaris and D2B instruments.

## 3. Results and discussion

Fig. 2 shows sintered ceramics of $Mn_{3-x}Co_xO_4$ observed by SEM after conventional and SPS processes. For the tetragonal phase prepared by the conventional method, the grain sizes are dispersed and vary from ~1 to 30 μm. The presence of aggregates in the raw powders can explain the grain size heterogeneity. For ceramics prepared by the SPS technique, the grain sizes vary from 0.1 to 0.7 μm. The lower sintering temperature (750 °C compared to ~1150 °C in the conventional route) and shorter heating time in the SPS process allow preserving the small grain size from the powders to the ceramics. The number of grain boundaries is larger and the ceramic densification higher after SPS treatment [22]. However, it is known that these differences observed in the NTC ceramic microstructures do not have a significant contribution in the conduction mechanisms [25]. Therefore, they will not be considered in this study.

Diffraction patterns of tetragonal ($x = 0.58$) and cubic ($x = 2.22$) spinels after Rietveld refinements are given as examples in Fig. 3. The cell variation of the single phase $Mn_{3-x}Co_xO_4$ ($0 \leq x \leq 3$) ceramics is represented in Fig. 4 and compared with X-ray data. The cell decrease with increasing *x* values in $Mn_{3-x}Co_xO_4$ thus leads to a compression of the empty octahedral sites. In the tetragonal structure, cations are located on the 4a tetrahedral site with (0, 0.25, 0.875) coordinates and 8d octahedral site with (0, 0.5, 0.5) coordinates, and anions on 16 h with $x = 0$. In the cubic spinel, cations are located on the 8a tetrahedral site with $x = y = z = -0.125$ and 16d octahedral site with $x = y = z = 0.5$, while anions occupy the 32e site. A small variation of the oxygen positions occurs in the tetragonal phase ($c/a'$ tends to 1, with $a' = \sqrt{2}.a_{tet}$), while a linear increase of the *u* value with increasing cobalt is observed in the cubic phase. The Co substitution drives to a progressive increase of the distance between the oxygen and its ideal position ($u = 0.25$), in agreement with the literature [26–28].

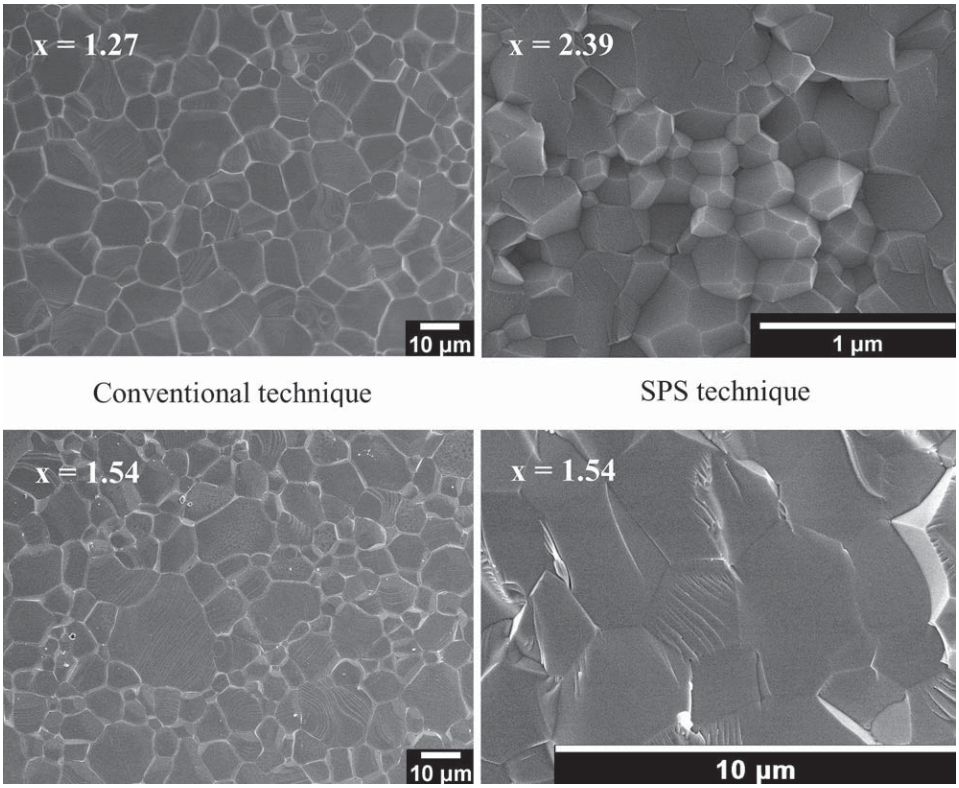


**Fig. 2.** Ceramics of $Mn_{3-x}Co_xO_4$ observed by SEM after conventional and SPS processes.

The oxygen thermal displacement parameter increases with cobalt up to the tetragonal/cubic transition limit then largely decreases until the $Co_3O_4$ composition. The strong structural distortion at the phase transition creates a large displacement of the oxygen around its average position. In the cubic phase, the increase of the *u* oxygen thermal displacement parameter is related to the cell parameter decrease due to the Co substitution in $Mn_{3-x}Co_xO_4$, and the space available for the free displacement of the oxygen atoms becomes smaller.

The shortest metal–metal distance variations are shown in Fig. 5a. There are two types of $[M_B–M_B]$ distances between adjacent octahedra connected by the edge in the tetragonal phase (one in the cubic spinel), two types of $[M_B–M_A]$ distances between adjacent octahedra and tetrahedra connected by corners (one in the cubic spinel) and one type of $[M_A–M_A]$ between closest tetrahedra (see Fig. 1). These intermetallic distances decrease in average when *x* varies from 0 to 3. In the oxide spinels, the electronic conduction takes place by hopping of polarons between cations with different oxidation states on an equivalent crystallographic site. Since the $[M_B–M_B]$ distances are the shortest, the electronic conduction will preferentially take place along the chains of octahedra.

The decrease of the $[M_B–M_B]$ distances with Co substitution over the whole solid solution range should favor the conductivity in those ceramics. However, the Mn-rich and Co-rich oxide spinel ceramics are strongly resistive. Other important factors such as the activation energy and the cation distribution on each site need to be considered for the understanding of the mechanisms of conduction in spinels.

The $[M_A–O]$ and $[M_B–O]$ average distances decrease while *x* increase in the tetrahedral and octahedral environments, respectively (see Fig. 5b). Considering the cation distribution $Mn^{2+}[Mn^{3+}]_2O_4$ for the haussmanite $Mn_3O_4$, the $[M_A–O]$ decrease with increasing *x* values can easily be explained by the $Co^{2+}$ substitution on the tetrahedral site. The $[M_B–O]$ decrease is due to the introduction of smaller cations in average on the octahedral site, $Co^{III}$ and/or ($Co^{2+}$ and $Mn^{4+}$) ions, which is also related to the cell diminishing observed in our ceramics. The tetragonal cell of $Mn_{2.42}Co_{0.58}O_4$ is strongly distorted due to the large amount of $Mn^{3+}$ on the octahedral site. The distortion implies an elongation of the $[M_B–O]_2$ distances along the *c*-axis and a decrease of the $[M_B–O]_1$ distances in the (*a*, *b*) planes. On the contrary, the lower concentration of $Mn^{3+}$ on octahedral site by Co substitution implies shorter $[M_B–O]_2$ distances and longer $[M–O]_1$ distances. For $x = 1.75$, the tetragonal to cubic transition is associated with an increase of symmetry and only one type of $[M_B–O]$ distances has to be considered in the Co-rich domain. The $[M_B–O]$ distances are in average larger than the $[M_A–O]$ distances for $0 \leq x \leq 2.22$ and become smaller for $x > 2.22$. For Co-rich manganese oxide spinels, the majority of $Co^{III}$ on the *B* site, with a smaller radius than the $Co^{2+}$ occupying the *A* site, could explain the shortest $[M_B–O]$ distances.

Neutron data refinements allowed us to identify the manganese and cobalt elements on each polyhedral site. Their proportions are given in Table 1 and the variation of the cobalt concentration on each site with composition is drawn in Fig. 6. Although our ceramics were quenched or quickly cooled down to room temperature, it can be clearly seen that the substitution of $Mn^{2+}$ by $Co^{2+}$ firstly occurs on the tetrahedral site for *x* increasing to 1 ($CoMn_2O_4$ composition). For further *x* values, $Co^{2+}$ and/or $Co^{III}$ are substituted into the octahedral sites, in accordance with the observed structural variations. The quenching temperature can have a strong influence on the degree of inversion and cation distribution in ceramics of $Mn_{3-x}Co_xO_4$ ($x \leq 1.75$). For instance, $c/a'$ ratio decreases by ~0.07 in $Mn_{1.75}Co_{1.25}O_4$ when this temperature increases by 100 °C and the cell is less distorted, in accordance with our X-ray data. The

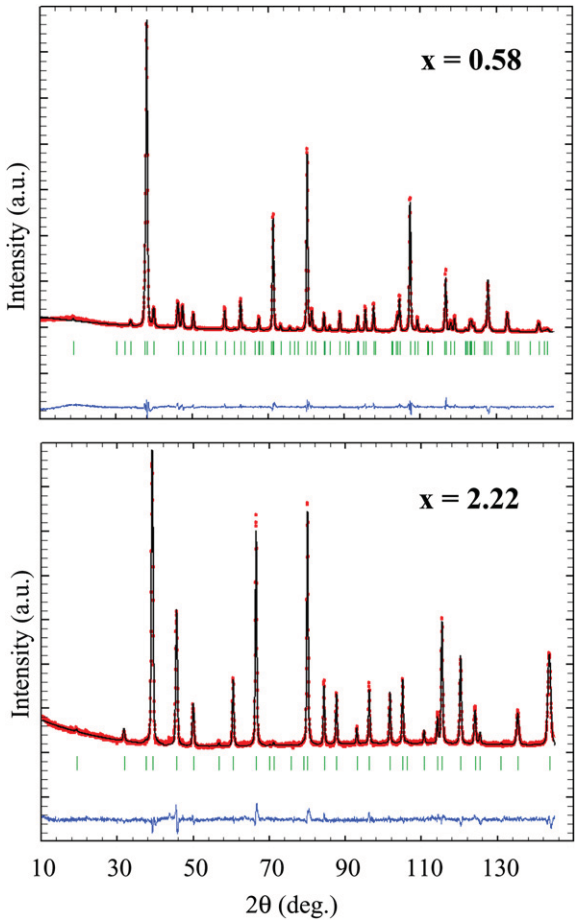


**Fig. 3.** Neutron diffraction patterns of $Mn_{3-x}Co_xO_4$ ceramics recorded on D2B ($\lambda = 1.594$ Å) after Rietveld refinements (observed = dots, calculated = lines, difference below). Reliability factors are: $R_p = 0.127$, $R_{wp} = 0.110$, $R_{exp} = 0.045$, $\chi^2 = 5.972$, $R_B = 0.053$, $R_F = 0.043$ (top) and $R_p = 0.147$, $R_{wp} = 0.107$, $R_{exp} = 0.069$, $\chi^2 = 2.389$, $R_B = 0.060$, $R_F = 0.042$ (bottom).

mechanisms of cation migration between the different crystallographic sites are activated and the concentration of $Mn^{3+}$ in octahedral site diminishes with the manganese ions being reduced and moving towards the tetrahedral sites. Inversely, the cobalt ions

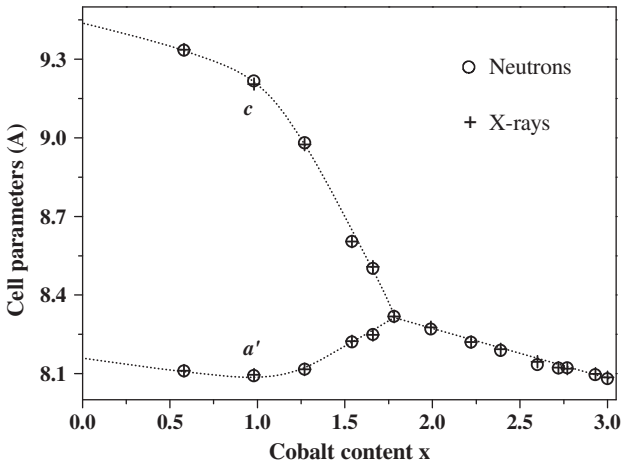


**Fig. 4.** Cell variation of $Mn_{3-x}Co_xO_4$ ceramics, with $0 \le x \le 3$, determined from neutron diffraction measurements. X-ray data is showed for comparison.

present on the tetrahedra tend to migrate to the octahedral environment (99% of Co on the *A* site and 26% of Co on the *B* site for a quenching temperature of 800 °C, while 80% of Co occupy the *A* site and 45% for the *B* site at 900 °C). These results confirm previous data published in the literature for $MnCo_2O_4$ [29] and remind us of the importance of the sample preparation method for determining its structural and physical properties. The lowering of the temperature before quenching a sample tends to stabilize the normal spinel. Closer to the transition composition, the effects of the quenching temperature are less obvious. For example, the cell parameters of $Mn_{1.46}Co_{1.54}O_4$ ceramics are almost identical and $c/a'$ ratio varies by only ~0.0008 for two different quenching temperatures (900 and 1180 °C). The influence of the quenching temperature over the cation organization of this compound is also very small with 90% (88%) and 64% (66%) on the tetrahedral and octahedral sites at 900 °C (1180 °C), respectively.

The determination of the cation distribution in cobalt and manganese oxide spinels is difficult due to the various possible oxidation states for both elements ($Mn^{2+}$, $Mn^{3+}$, $Mn^{4+}$ and $Co^{2+}$, $Co^{III}$, $Co^{4+}$). To our knowledge, the presence of $Co^{4+}$ ions has mainly been reported in perovskite structural types of materials and only very exceptionally in spinel compounds [30,31]. We will not consider this oxidation state for the cobalt in our study. The remaining cations could theoretically occupy randomly either sites in our oxide spinels. However, thermodynamic considerations have shown that $Co^{III}$, $Mn^{3+}$ and $Mn^{4+}$ are usually positioned on octahedral sites, while $Mn^{2+}$ and $Co^{2+}$ have no preference [20,32]. Regarding the cation radii and [M–O] distances referenced in the literature for the two types of environment considered here, we have been able to use our neutron data for the determination of the cation distributions in $Mn_{3-x}Co_xO_4$ over the whole solid solution range.

For $0 \le x \le 1$, our preliminary structural studies showed that $Mn^{2+}$ was progressively replaced by $Co^{2+}$ on the tetrahedral site, and $Mn^{2+}[Mn^{3+}{}_2]O_4$ tends to $Co^{2+}[Mn^{3+}{}_2]O_4$, in accordance with previous results obtained in powders [33,34].

For $1 < x \le 3$, considering that the tetrahedral sites are fully occupied by $Co^{2+}$, the adding cobalt element will then occupy the octahedral sites as $Co^{2+}$ and/or $Co^{III}$. Three alternatives can thus be considered: (i) the introduction of $Co^{2+}$ in the *B* site is associated with the presence of $Mn^{3+}$ and $Mn^{4+}$ for preserving the global electroneutrality. Using the 55% critical amounts of distorting $Mn^{3+}$ required in this site for the tetragonal distortion of the spinel to occur, the structural transition should take place between $x = 1.25$ and 1.54 for such cation distribution. Experimentally, this transition occurs for $x \sim 1.75$. Therefore, this cation distribution was excluded; (ii) the progressive replacement of $Mn^{3+}$ by $Co^{III}$ in the octahedral site is the usual substitution process taken into account in the literature, especially for $MnCo_2O_4$ [26,33,35]. In this case, the proportion of each cation calculated as a function of composition shows that the critical concentration of distorting cations in the *B* site would be for an *x* value well above 1.75, which is contrary to our experimental results. TGA measurements performed on synthetic powders of cobalt and manganese oxide spinels confirmed this conclusion; (iii) the simultaneous substitution of $Mn^{3+}$ by $Co^{2+}$ and $Co^{III}$ in the octahedral site is accompanied by the partial oxidation of $Mn^{3+}$ to $Mn^{4+}$. Thus, neutron data were used for proving that the latter hypothesis must be the only possible explanation for the structural and physical variations observed in our ceramics. In order to determine the cation concentrations on the *B* sites we used two structural methods.

First, following Poix's work on orthotitanate and orthostanate spinels [36,37] we used the relation between a theoretical cell parameter and the average [$M_A$–O] and [$M_B$–O] distances calculated for each site.

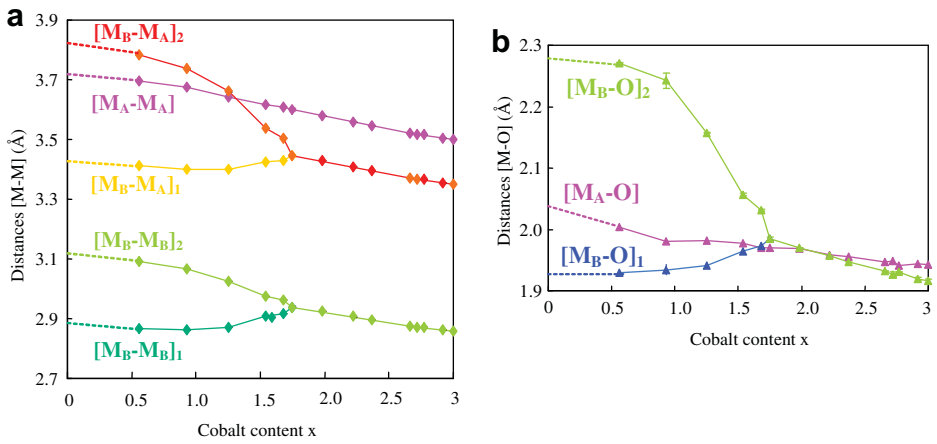


**Fig. 5.** a) Metal–Metal and b) Metal–Oxygen distance variations in $Mn_{3-x}Co_xO_4$ ceramics ($0 \leq x \leq 3$).

It was then possible to compare the experimental cell parameter with the theoretical value for a given cation distribution. Inversely, the cation distribution can be determined starting from the experimental $c_{exp}$ cell value by:

$$[M_B - O]_{moy} = \sqrt{\frac{c_{exp}^2 - 4,199 \cdot c_{exp} \cdot [M_A - O]_{moy} + 2,9972 \cdot [M_A - O]_{moy}}{5,8182}}$$

with:

$$[M_A - O]_{moy} = \sum_i x_i \cdot [M - O]_i \text{ and } [M_B - O]_{moy} = \frac{1}{2} \cdot \sum_j y_j \cdot [M - O]_j$$

$x_i$, $y_j$: concentrations of i and j ions in the *A* and *B* sites, respectively [38].

$[M–O]_i$, $[M–O]_j$: Metal–Oxygen distances for a cation at a chosen oxidation state in the *A* and *B* sites, respectively [36,37].

In the tetragonal phase, we used a $c'_{exp}$ cell parameter defined by: $c'_{exp} = 3\sqrt{a'^2_{exp} \cdot c_{exp}}$

The average $[M_A–O]$ distance was calculated by using the $Co^{2+}$ and $Mn^{2+}$ ion concentrations determined for the *A* site after the neutron data refinements. The cation distribution in the *B* site obtained for each composition is shown in Table 2. For $x \geq 1.25$, the amount of $Co^{III}$ in octahedral site increases almost linearly with *x*, while $Mn^{3+}$ concentration decreases. The $Co^{2+}$ and $Mn^{4+}$ concentrations, equivalent for electroneutrality, slowly increase up to $x \sim 2.22$, where the maximum proportion of both ions in octahedral site is ~16%, then decrease until the $Co_3O_4$ composition. For the pure cobalt oxide spinel ceramic prepared by SPS technique, an inversion of the normal spinel due to the presence of $Co^{2+}$ ions in the *B* site was observed. Although the normal spinel configuration is usually adopted by $Co_3O_4$, previous thermodynamic and structural studies showed that $Co^{2+}$ and $Co^{III}$ can both occupy randomly the *A* and *B* sites at high temperature [39,40]. The structure of $Co_3O_4$ is then disordered and the cobalt ions can adopt the high and low-spin configurations with a small cell increase due to a higher $Co^{3+}$ radius in comparison with the $Co^{III}$ ion. This assumption was confirmed by the electrical measurements showing that $Co_3O_4$ ceramics were rather semiconductors than insulators with a resistivity value of $\sim 3.4 \times 10^3\ \Omega$ cm at room temperature. The

**Table 1**
Cobalt and manganese concentrations on the tetrahedral (*A*) and octahedral (*B*) sites of $Mn_{3-x}Co_xO4$ ($0 < x \leq 3$) ceramics.

| *x* | Co (*A* site) | Mn (*A* site) | Co (*B* site) | Mn (*B* site) |
|---|---|---|---|---|
| 0.58 | 0.58(1) | 0.42(1) | 0.00(1) | 2.00(1) |
| 0.93 | 0.92(1) | 0.08(1) | 0.01(2) | 1.99(2) |
| 1.25 | 0.99(1) | 0.01(1) | 0.26(1) | 1.74(1) |
| 1.54 | 0.90(1) | 0.10(1) | 0.64(1) | 1.36(1) |
| 1.67 | 0.92(1) | 0.08(1) | 0.75(1) | 1.25(1) |
| 1.75 | 0.969(9) | 0.031(9) | 0.782(9) | 1.218(9) |
| 1.98 | 0.965(7) | 0.035(7) | 1.011(7) | 0.989(7) |
| 2.22 | 0.971(5) | 0.029(5) | 1.249(4) | 0.751(4) |
| 2.37 | 0.973(4) | 0.027(4) | 1.395(2) | 0.605(2) |
| 2.66 | 1.000(9) | 0.000(9) | 1.656(8) | 0.344(8) |
| 2.72 | 1.000(6) | 0.000(6) | 1.718(3) | 0.282(3) |
| 2.76 | 0.994(3) | 0.006(3) | 1.765(3) | 0.235(3) |
| 2.92 | 0.998(3) | 0.002(3) | 1.924(3) | 0.076(3) |
| 3 | 1.000(1) | 0.000(1) | 2.000(1) | 0.000(1) |

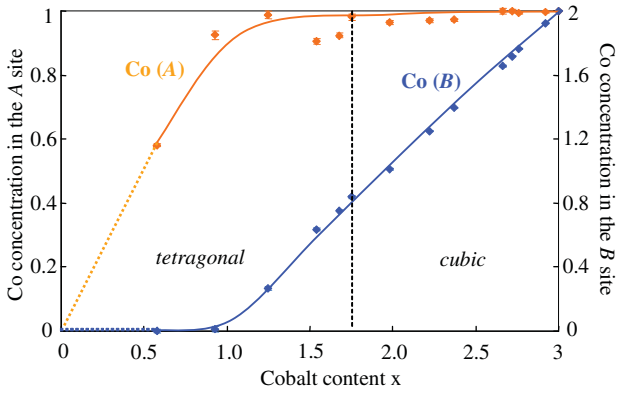


**Fig. 6.** Variations of the cobalt concentrations on the *A* and *B* sites for $Mn_{3-x}Co_xO_4$ ceramics.

**Table 2**
Variation of the cation concentrations on the *B* sites for $Mn_{3-x}Co_xO_4$ ($1 < x \leq 3$) ceramics determined by the structural method based on Poix's previous studies [36,37] and using neutron data. The values deviations based on the uncertainties given by the FULLPROF program for each crystallographic site are about 2%.

| *x* | $Co^{2+}$ | CoIII | $Mn^{3+}$ | $Mn^{4+}$ |
|---|---|---|---|---|
| 1.25 | 0.06 | 0.20 | 1.68 | 0.06 |
| 1.54 | 0.08 | 0.56 | 1.28 | 0.08 |
| 1.67 | 0.10 | 0.65 | 1.15 | 0.10 |
| 1.75 | 0.11 | 0.67 | 1.11 | 0.11 |
| 1.98 | 0.21 | 0.80 | 0.78 | 0.21 |
| 2.22 | 0.33 | 0.92 | 0.42 | 0.33 |
| 2.37 | 0.26 | 1.13 | 0.35 | 0.26 |
| 2.66 | 0.25 | 1.41 | 0.09 | 0.25 |
| 2.72 | 0.24 | 1.48 | 0.04 | 0.24 |
| 2.76 | 0.21 | 1.55 | 0.03 | 0.21 |
| 2.92 | 0.07 | 1.85 | 0.01 | 0.07 |
| 3 | 0.13 | 1.87 | 0 | 0.13 |

electronic conduction is then enhanced by the presence of $Co^{2+}$ and $Co^{III}$ and/or $Co^{3+}$ on the octahedral sites with a low activation energy value ($E_a = 0.25$ eV), in agreement with results reported in the literature for ceramics of $Co_3O_4$ [41].

Second, the bond valence sum (BVS) calculations were performed using the neutron data and the FULLPROF program [24,42–44]. Only $Co^{2+}$ on tetrahedral sites were considered before BVS calculations, except for $x = 1.54$ and 1.67 where the manganese concentration was about 9%. The first refinements made by taking only $Co^{III}$ and $Mn^{3+}$ into account on the *B* site showed a difference of ±0.4 compared to the initial charge value, suggesting the presence of other types of cations in octahedral environments as evidenced before. Therefore, the BVS calculations were realized with four different cations on the *B* site ($Co^{2+}$, $Co^{III}$, $Mn^{3+}$ and $Mn^{4+}$) for each $Mn_{3-x}Co_xO_4$ composition ($1.25 \leq x \leq 3$). The individual bond valence sums obtained for two cations of a same element were averaged to the equivalent charge of the element to calculate the cation concentrations on the octahedral site (Table 3). The average oxidation state determined for the *B* site was then always close to 3.00(8). Although the $Co^{2+}$ and $Mn^{4+}$ were independently refined by the BVS calculations, the results showed a similar trend for both concentrations and the variations of the cation distributions with composition using the two methods of calculation were generally very close.

Finally, we compared the cation distributions determined in our ceramics with TGA analyzes performed on the $Mn_{3-x}Co_xO_4$ powders ($1.99 \leq x \leq 3$) used for preparing the ceramics (data to be published) [45]. For each composition of cubic spinel structure obtained at room temperature and measured in air up to 1300 °C, two steps of decomposition were observed, corresponding to the

**Table 3**
Average bond valence sums for the cobalt, manganese and oxygen elements, and cation concentrations on the *B* sites for $Mn_{3-x}Co_xO4$ ($1 < x \leq 3$) ceramics determined by the BVS method and the FULLPROF program.

| *x* | $\Sigma v_i$(Co) | $\Sigma v_i$(Mn) | $\Sigma v_i$(O) | $Co^{2+}$ | CoIII | $Mn^{3+}$ | $Mn^{4+}$ |
|---|---|---|---|---|---|---|---|
| 1.25 | 2.431 | 3.109 | 1.93 | 0.13 | 0.13 | 1.55 | 0.19 |
| 1.54 | 2.480 | 3.171 | 1.95 | 0.33 | 0.31 | 1.21 | 0.15 |
| 1.67 | 2.502 | 3.200 | 1.95 | 0.37 | 0.38 | 1.00 | 0.25 |
| 1.75 | 2.804 | 3.234 | 1.95 | 0.15 | 0.63 | 0.93 | 0.29 |
| 1.98 | 2.635 | 3.370 | 1.98 | 0.37 | 0.64 | 0.62 | 0.37 |
| 2.22 | 2.727 | 3.488 | 1.98 | 0.34 | 0.91 | 0.38 | 0.37 |
| 2.37 | 2.807 | 3.590 | 2.00 | 0.27 | 1.12 | 0.25 | 0.36 |
| 2.66 | 2.917 | 3.730 | 2.04 | 0.14 | 1.52 | 0.09 | 0.25 |
| 2.72 | 2.960 | 3.780 | 2.04 | 0.07 | 1.65 | 0.06 | 0.22 |
| 2.76 | 2.960 | 3.780 | 2.03 | 0.07 | 1.69 | 0.05 | 0.19 |
| 2.92 | 3.017 | 3.859 | 2.00 | 0.04 | 1.88 | 0.01 | 0.07 |
| 3 | 3.055 | | 1.92 | 0.34 | 1.66 | | |

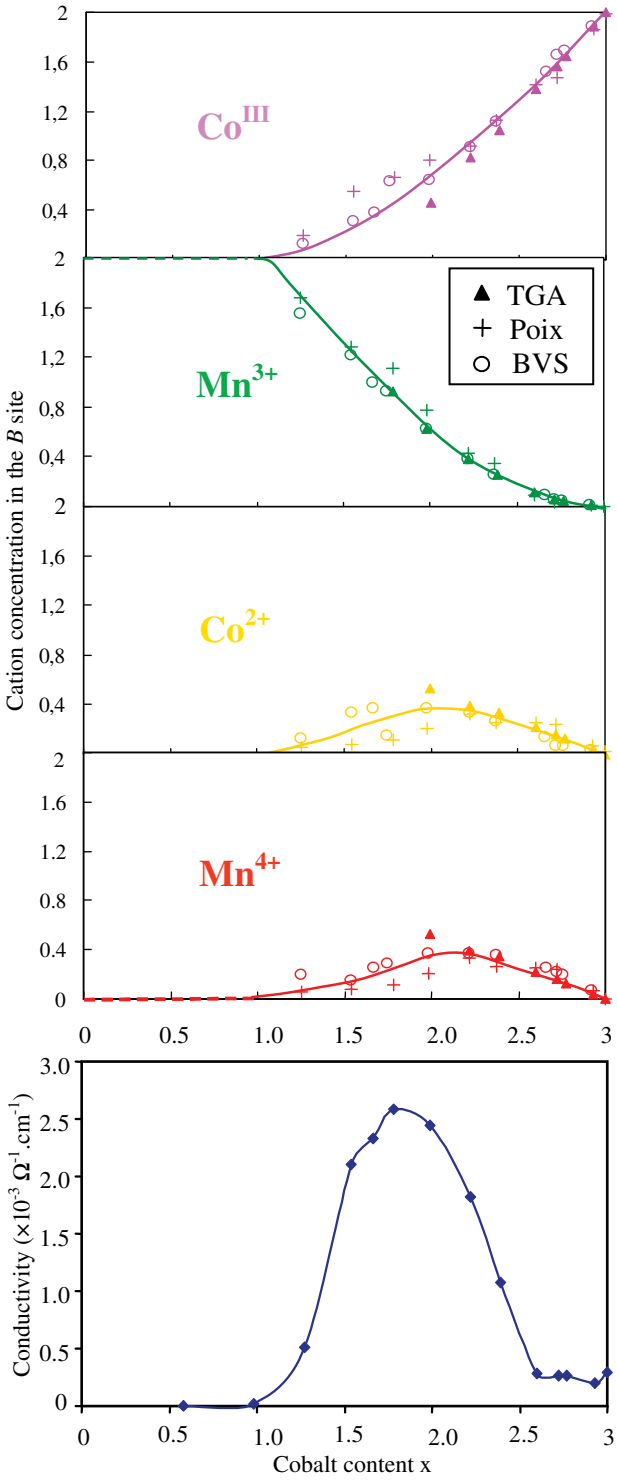


**Fig. 7.** Cation distribution in $Mn_{3-x}Co_xO_4$ ceramics ($0 \leq x \leq 3$) determined by the structural methods following Poix's work [36,37] and the Bond Valence Sum (BVS) calculations. TGA data obtained on powders for $2 \leq x \leq 3$ and conductivity variations are represented for comparison.

reduction of $Co^{III}$ to $Co^{2+}$ followed by the reduction of $Mn^{4+}$ to $Mn^{3+}$. These results confirmed the general tendencies observed in the variation of the cation concentrations with composition and deduced from the neutron data. Fig. 7 summarizes the cation distribution variations in the *B* site of $Mn_{3-x}Co_xO_4$ determined by the three methods over the whole solid solution. The variation of

conductivity with the cobalt content is also given in Fig. 7 for comparison. It shows that a maximum of conductivity is reached when $Mn_{3-x}Co_xO_4$ ceramics present a large number of $Co^{2+}/Co^{III}$ and $Mn^{3+}/Mn^{4+}$ couples on the octahedral site (with $[Co^{III}] \sim [Mn^{3+}]$ and $[Co^{2+}] \sim [Mn^{4+}]$). This important information may suggest that the electrical conduction in cobalt and manganese oxide spinels results essentially from a coupled polaron hopping mechanism between adjacent $Mn^{3+}/Mn^{4+}$ and $Co^{2+}/Co^{III}$ on the *B* sites.

## 4. Conclusions

For the first time to our knowledge, structural variation and cation distribution in cobalt manganese oxide spinels have been determined for ceramics over the whole solid solution range. Rietveld refinements of neutron data obtained at room temperature on our single phase ceramics proved that the tetragonal (for $x < 1.75$) and cubic (for $x \geq 1.75$) cells decrease with cobalt substitution for manganese. The [M–M] hopping distances, shorter between near octahedra connected by edges, also decrease in average. However, this information can not explain in itself the conductivity variation observed in the oxide spinels since the highest conductivity values are measured for $1.5 < x < 2$. Structural studies applied to the whole $Mn_{3-x}Co_xO_4$ system, essentially based on neutron data and experimental [M–O] distances compared with tabulated values, show that $Mn^{2+}$ on tetrahedral sites are progressively replaced by $Co^{2+}$ for *x* varying from 0 to 1, then $Mn^{3+}$ on octahedral sites are substituted by $Co^{2+}$, $Co^{III}$ and $Mn^{4+}$ for $1 < x < 3$.

The substitution process can be schematized as follows:

$$0 \leq x \leq 1, \qquad Mn^{2+}[Mn_2^{3+}]O_4^{2-}$$
$$\rightarrow Co^{2+}{}_xMn_{1-x}^{2+}[Mn_2^{3+}]O_4^{2-}$$
$$\rightarrow Co^{2+}[Mn_2^{3+}]O_4^{2-}$$

$$1 < x \leq 3, \qquad Co^{2+}[Mn_2^{3+}]O_4^{2-}$$
$$\rightarrow Co^{2+}[Co_y^{2+}Co^{III}{}_{x-y-1}Mn_{3-x-y}^{3+}Mn^{4+}{}_y]O_4^{2-}$$
$$\rightarrow Co^{2+}[Co_2^{III}]O_4^{2-}, \text{with } 0 \leq y \leq 0.40.$$

The novel cation distribution found in the cubic phase was also justified by TGA measurements performed on powders of $Mn_{3-x}Co_xO_4$. For manganese-rich oxide spinels, we showed that the quenching temperature used for sintering our ceramics has a strong influence on the element proportions on each site and cobalt can start to appear on the octahedra before filling up completely the tetrahedral site. On the other end, $Co_3O_4$ sintered by SPS technique exhibits some cation disorder that we believe is due to the presence of $Co^{2+}$ and $Co^{III}/Co^{3+}$ on the octahedral site that favors the electronic conduction through the ceramics.

The relationships between the structural and electrical properties of the cobalt manganese oxide spinels described here should be of high interest in the comprehension of the conduction mechanisms involved in such compounds. Spectroscopy techniques such as XAFS, EPR… are envisaged for the confirmation of the cation oxidation and spin states in these complex samples. Further studies on their electrical and magnetic properties are currently underway in order to compare them with other manganese-based oxide spinels. These cobalt and manganese oxide spinel ceramics can be used for future commercial applications as NTC in microelectronic devices and other integrated systems.

## Acknowledgments

The authors wish to thank the Vishay BCcomponents Company and the CNRS for financial supports. Gilles Andre from the LLB at Saclay, Thierry Roisnel from the University of Rennes and Juan-Rodriguez-Carvajal from the ILL at Grenoble are gratefully acknowledged for their very interesting comments on the neutron data and BVS calculations.

## Appendix. Supplementary data

The supplementary materials can be viewed at doi:10.1016/j.solidstatessciences.2009.11.018.

## References

[1] J.L. Martin de Vidales, P. Garcia-Chain, R. Rojas, E. Vila, O. Garcia-Martinez, J. Mater. Sci. 33 (1998) 1491.
[2] T. Yokoyama, T. Meguro, Y. Shimada, J. Tatami, K. Komeya, Y. Abe, J. Mater. Sci. 42 (2007) 5860.
[3] E.H. Jabry, A. Rousset, A. Lagrange, Phase Transitions 13 (1988) 63.
[4] A. Feltz, J. Topfer, F. Schirrmeister, J. Eur. Ceram. Soc. 9 (1992) 187.
[5] S.T. Kshirsagar, C.D. Sabane, Jpn. J. Appl. Phys. 10 (1971) 794.
[6] J.L. Gautier, S. Barbato, J. Brenet, C.R. Acad. Sci. Paris 294 (1982) 427.
[7] G.P. Vasil'ev, L.A. Pakhomov, L.A. Ryabova, Thin Solid Films 66 (1980) 119.
[8] N. Yamamoto, S. Higashi, S. Kawano, N. Achiwa, J. Mater. Sci. Lett. 2 (1983) 525.
[9] G. Blasse, Philips Res. Rep. 18 (1963) 383.
[10] A. Restovic, E. Rios, S. Barbato, J. Ortiz, J.L. Gautier, J. Electroanal. Chem. 522 (2002) 141.
[11] H. Eba, K. Sakurai, J. Solid State Chem. 178 (2005) 370.
[12] C.D. Spencer, D. Schoeer, Phys. Rev. B 9 (1974) 3658.
[13] M. Lenglet, B. Lefez, Solid State Commun. 98 (1996) 689.
[14] D. Jarosch, Miner. Petrol. 37 (1987) 15.
[15] H.A. Jahn, E. Teller, P. Roy, Soc. A-Math. Phys. 161 (1937) 220.
[16] N. Baffier, M. Huber, J. Phys. Chem. Solids 33 (1972) 737.
[17] A.S. Borovik-Romanov, M.P. Orlova, Sov. Phys. JETP 5 (1957) 1023.
[18] E.J.W. Verwey, E.L. Heilmann, J. Chem. Phys. 15 (1947) 174.
[19] E.J.W. Verwey, F.D. Boer, J.H.V. Santen, J. Chem. Phys. 16 (1948) 1091.
[20] A. Navrotsky, O.J. Kleppa, J. Inorg. Nucl. Chem. 29 (1967) 2701.
[21] H.S.C. O'Neill, A. Navrotsky, Am. Mineral. 68 (1983) 181.
[22] H. Bordeneuve, S. Guillemet-Fritsch, A. Rousset, S. Schuurman, V. Poulain, J. Solid State Chem. 182 (2009) 396.
[23] E. Aukrust, A. Muan, Trans. Metal. Soc. Aime 230 (1964) 378.
[24] J. Rodriguez-Carvajal, Physica B 92 (1993) 55.
[25] R. Metz, R. Legros, A. Rousset, J.P. Caffin, A. Loubière, A. Bui, Silic. Ind. 3-4 (1990) 71.
[26] B. Boucher, R. Buhl, R. Di Bella, M. Perrin, J. de Physique 31 (1970) 1139.
[27] W.L. Roth, J. Phys. Chem. Solids 25 (1964) 1.
[28] O. Knop, I.G. Reid, Y. Sutarno, Y. Nakagawa, Can. J. Chem. 46 (1968) 3463.
[29] R. Buhl, J. Phys. Chem. Solids 30 (1969) 805.
[30] S.R. Sehlin, H.U. Anderson, D.M. Sparlin, Phys. Rev. B 52 (1995) 11681.
[31] G.V. Bazuev, O.I. Gyrdasova, Phys. Status Solidi B 245 (2008) 1184.
[32] A. Navrotsky, J. Inorg. Nucl. Chem. 31 (1969) 59.
[33] D.G. Wickham, W.J. Croft, J. Phys. Chem. Solids 7 (1958) 351.
[34] K.S. Irani, A.P.B. Sinha, A.B. Biswas, J. Phys. Chem. Solids 23 (1962) 711.
[35] S. Naka, M. Inagaki, T. Tanaka, J. Mater. Sci. 7 (1972) 441.
[36] P. Poix, Bull. de la Société Chimique de France 5 (1965) 1085.
[37] P. Poix, C.R. Acad. Sci. Paris 268 (1969) 1139.
[38] M. Laarj, S. Kacim, B. Gillot, J. Solid State Chem. 125 (1996) 67.
[39] H.S.C. O'Neill, Phys. Chem. Miner. 12 (1985) 149.
[40] X. Liu, C.T. Prewitt, Phys. Chem. Miner. 17 (1990) 168.
[41] E.W. Gorter, Philips Res. Rep. 9 (1954) 295.
[42] I.D. Brown, D. Altermatt, Acta Cryst. B 41 (1985) 244.
[43] R.M. Wood, G.J. Palenik, Inorg. Chem. 37 (1998) 4149.
[44] N.E. Brese, M. O'Keeffe, Acta Cryst. B 47 (1991) 192.
[45] H. Bordeneuve, A. Rousset, C. Tenailleau, S. Guillemet-Fritsch, J. Therm. Anal. Calorim. doi:101007/s10973-009-0557-7.